

Study of the Cygnus X-3 Microquasar with the RATAN-600 Radio telescope in Multi-Azimuth Observing Mode

S. A. Trushkin,^{1,2,*} A. V. Shevchenko,¹ N. N. Bursov,¹ P. G. Tsybulev,¹
N. A. Nizhel'skii,¹ A. N. Borisov,¹ A. A. Kudryashova¹

¹*Special Astrophysical Observatory, Russian Academy of Sciences, Nizhnii Arkhyz, 369167 Russia*

²*Kazan (Volga Region) Federal University, Kazan, 420008 Russia*

We have been performing daily observations of bright microquasars at 1.2–20 GHz with the Northern sector of RATAN-600 radio telescope for more than ten years. During the 2019–2021 observations we recorded bright flares, which we call giant flares because fluxes reach record levels—above 20 Jy—during these events. In this paper we report the results of intraday variations of the Cygnus X-3 microquasar in multi-azimuth observations made with the “North sector with a flat-sheet reflector” during giant flares of Cygnus X-3. These were the first such observations made simultaneously at several frequencies on a short time scale (10 minutes). Observational data consists of 31 measurement made within ± 2.7 hours of the culmination of the object. We are the first to discover the evolution of the spectrum of the flare emission of Cygnus X-3 on a time scale comparable to the orbital period of the binary. The measurement data allowed us to determine the temporal and spectral parameters of radio emission, which are typical for synchrotron flare emission in relativistic jets. Evolution of the radio emission of X-ray binaries on short time scales is a key to understanding the formation of jet outbursts in the process of mass accretion of the matter of the donor star onto the relativistic object.

Ключевые слова: stars: individual: Cygnus X-3—ISM: jets and outflows—radio continuum: stars

1. INTRODUCTION

The Cygnus X-3 X-ray binary—a microquasar with relativistic jets—consists of a massive Wolf-Rayet star (van Kerkwijk et al., 1992) and a compact object (a black hole or a neutron star). The orbital period of this system determined from IR and X-ray data is 4.8 hours (Bhargava et al., 2017), i.e., the system is very compact and strong wind from the donor star is one of the key factors influencing the features of jet outflows during bright flares. The object was found to be an X-ray object in 1967 (Giacconi et al., 1967), and powerful radio flares of Cygnus X-3 have been observed since 1972 when the properties of variable radio emission were discussed in detail in a series of 22 papers published in “Nature” (see Gregory et al. (1972)). long-term monitoring In the 1980s–1990s long-term monitoring of radio emission was produced with the NRAO interferometer (USA) (Waltman et al., 1994, 1996). After the launch of X-ray space observatories with daily monitoring programs (RXTE, BATSE, Swift) it became clear

that radio flares and X-ray flux are strongly correlated in all microquasars (McCollough et al., 1999). This property was named “coupling” of different processes in X-ray binaries that ensure mass accretion onto the relativistic object. This also fully applies to Cygnus X-3, for which the X-ray “hardness–intensity” evolutionary dependence resembling, on the whole, similar diagrams for other X-ray binaries with accreting black holes (Koljonen et al., 2010). There is a molecular cloud on the Cygnus X-3 line of sight, which causes strong absorption in the visible preventing optical spectroscopy. The object is at the distance of 7.2 kpc. Gamma-ray flux of Cygnus X-3 also correlates with the radio flare activity (Tavani et al., 2009; Corbel et al., 2012) and it is studied extensively by Fermi/LAT and AGILE space observatories. Zdziarski et al. (2018) did a detailed analysis of simultaneous radio (AMI-LA) and gamma-ray (Fermi/LAT) measurements. Both types of measurements were found to exhibit a weak flux modulation with the orbital period. The object has been VLBI mapped repeatedly with observations revealing jet outflows with relativistic jet

* sergei.trushkin@gmail.com

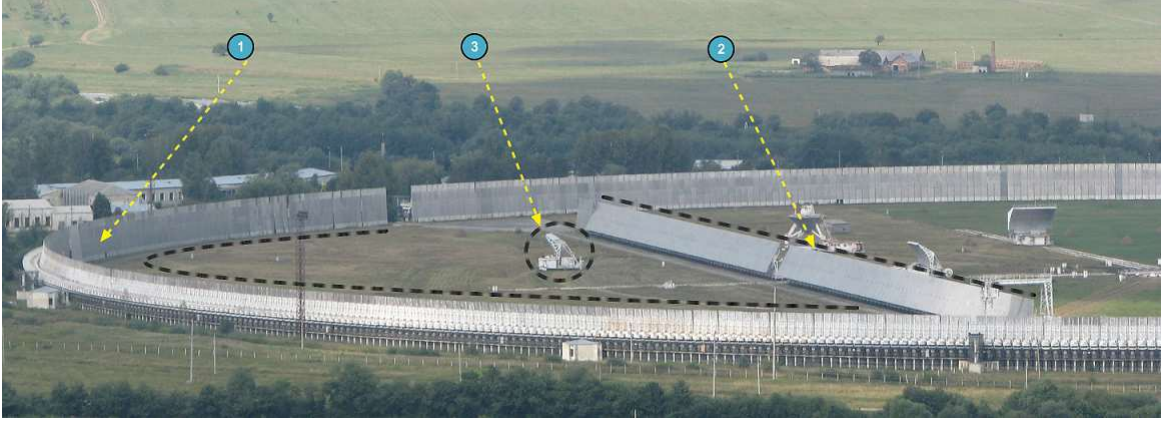


Figure 1. The “Southern sector with a flat reflector” antenna system of RATAN-600 radio telescope. (1)—Southern sector of the antenna, (2)—Flat-sheet reflector, (3)—secondary (third) reflector of the feed cabin.

motions *s* (Miller-Jones et al., 2004; Tudose et al., 2007). Such motions were in some cases interpreted as “superluminal”, which can most likely be explained as motion in jets directed at small angles to the line of sight (Spencer, 1998). It is evident that the time scale of variability also shortens in this case.

Cygnus X-3 stands out among microquasars by its occasional giant radio flares when flux may increase in few days by factors of several thousand that occur compared to the pre-flare level (Waltman et al., 1996). These giant flares occur immediately after the end to the state of almost complete “quenching”, i.e., after the 4–11 GHz radio flux has remained below 5–20 mJy for one to three weeks (Trushkin et al., 2017). Such a period of low radio flux is also characterized by a hypersoft X-ray state during which hard X-ray flux (15–50 keV) drops to zero, whereas the level of soft X-ray flux (< 15 keV) remains high or even increases (Koljonen et al., 2010). In such a state relativistic radio jets probably disappear completely. The intraday variability of Cygnus X-3 has been detected repeatedly, especially at millimeter- and centimeter-wave frequencies, which is not surprising given that the compact size of the system, relativistic nature of jets, and small absorption of radio emission. However, simultaneous multi-frequency measurements are of special interest for a detailed comparison and search for new patterns.

2. MULTI-AZIMUTH OBSERVATION MODE

Observations were made with a three-mirror system “Southern sector with a flat reflector” (Fig. 1). This antenna configuration allows a cosmic source to be monitored by changing the azimuth of the parabolic southern sector within $\pm 30^\circ$, and the elevation of the flat mirror and azimuth of the third mirror within $\pm 30^\circ$.

The third mirror can relatively rapidly move along arch rails with radius of about 150 m, which allows changing the azimuth of the antenna focus and thereby track the source in the sky. In 2018 three radiometers operating in the 4.7, 8.6, and 16 GHz frequency ranges were mounted in the focal plane of the third mirror (see Table 1).

In 2019 one of the radiometers of the facility of sensitive 4.7 GHz four-channel detectors operating in the full-power mode and used to search for rapid radio flares was temporarily mounted in the focal plane of the third mirror. The broad 600 MHz-wide bandwidth of each radiometer was subdivided into four narrow 150-MHz wide subbands. At the output of each narrow channel ADC were installed after the quadratic detector to record digital signals. In these measurements signals in the narrow detectors of this radiometer were averaged in the process of reduction of observations. This detector replaced the previous one at 4.7 GHz because it provided higher sensitivity throughout a broader bandwidth.

Table 1. Parameters of radiometer facilities. Designations: ν —the central frequency (GHz); $\Delta\nu$ —the bandwidth (GHz); ΔS_ν —the sensitivity in terms of flux per resolution beam (mJy/beam), and Phi05—the halfwidth of the antenna beam in arcseconds for the transit of a source at the declination of $\delta \sim 42^\circ$

ν , GHz	$\Delta\nu$, GHz	ΔS_ν , mJy/beam	Phi05, arcsec
Northern sector			
4.7	0.6	5	48
8.2	1	10	30
11.2	1.4	15	21
21.7	2.5	50	15
Southern sector with a flat reflector			
4.7*	0.6	10	72
4.7	0.6	10	72
8.6	1.4	20	39
16	2	60	30

*—four-beam facility

The discrete setting of the antenna with a step of 2° in azimuth made it possible to make 31 measurement of the object, which in the case of Cygnus X-3 was implied 10-minute intervals between the measurements. The apparent positions of the sources were computed using EFRAT ephemeris program developed at the Main Astronomical Observatory of the Russian Academy of Sciences specifically for the use on RATAN-600 telescope (Korzhavin et al., 2012).

The working EFRAT program is available from the RATAN-600 server and it is routinely used for solar measurements and for measurements of other Solar-system planets. The basic antenna parameters (effective area and beam size) were measured during observations of calibrating sources (Fig. 2 and Fig. 3). The antenna efficiency decreases appreciably at extreme azimuths because of the reduction of the aperture of the Southern sector, which is limited to one quarter of the circular reflector of RATAN-600. The beam size along the trajectory of the source transit through fixed beam varied because of the change of the parallax angle. The vertical beam size also varied, from $37'$ at the meridian to $50'$

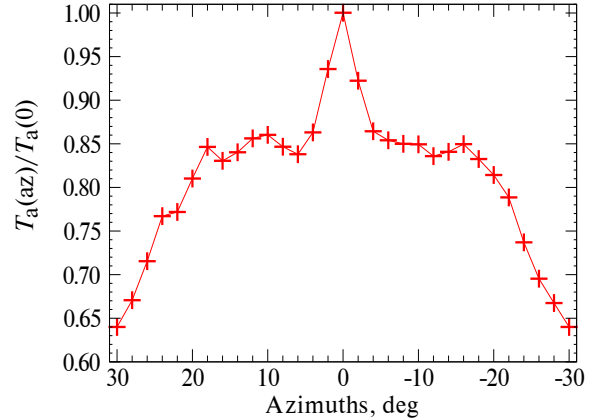


Figure 2. Dependence of normalized antenna temperatures of NGC 7027 on the azimuth of the “Southern sector with a flat reflector” antenna system.

at $\pm 30^\circ$ azimuths.

We employed the routine RATAN-600 procedure for full-power radiometers for daily monitoring of Cygnus X-3 at the meridian, its detailed review can be found in Tsybulev et al. (2018). Low-noise HEMT transistor based amplifiers are mounted on all radiometers.

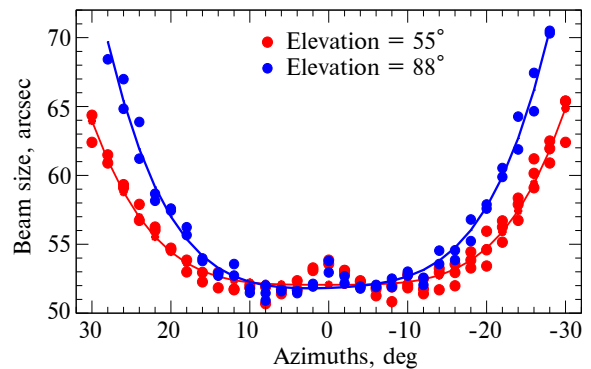


Figure 3. Size of the cross sections of the “Southern sector with a flat reflector” multi-azimuth antenna system for two sources at two different declinations.

Flux calibration in multi-azimuth mode was performed by observing the bright radio galaxy NGC 1275 (3C 84, J0319+41), planetary nebula NGC 7027 (J2107+42), and the H II region DR 21 (J2039+42). Observations of calibrating sources at close declinations were performed similarly to observations of the microquasar studied thereby providing accurate flux calibration and control of antenna parameters at different

azimuths. The calibrating sources were observed several times during the entire cycle of Cygnus X-3 intraday observations. The radio spectrum of J0319+41 was preliminary measured in observations with the Northern sector and the measured fluxes were converted into the fluxes at the frequencies used in multi-azimuth mode. We adopted the NGC 7027 and DR 21 fluxes in accordance with precision measurements by Ott et al. (1994) taking into account the secular flux decrease due to the expansion of the NGC 7027 shell. Our experience with observations of reference sources suggests that the total flux calibration error is not greater than 3%.

We reduced our observational data using FADPS software (Verkhodanov, 1997). To increase the S/N ratio, when reducing the data we convolved observational records with the computed beam pattern of RATAN-600 or with the drift scans of bright reference sources. The accuracy of flux measurements at levels higher than 1 Jy was better than 3% at 4.7 GHz and about 5–10% at 8.6 and 16 GHz. The error of the measured spectral index on the plots of variation of this parameter was ± 0.05 or higher. The high measurement accuracy at 4.7 GHz was due to high flux values during flares, i.e., the signal exceeded noise by several factors of ten. That is why the error bars in light-curve plots are smaller than the flux value signs.

Summary Table 2 lists the data of Cygnus X-3 multi-azimuth observations and the reference sources used in observations. During the date intervals mentioned in the table the Cygnus X-3 monitoring program was carried out daily on the Northern sector.

3. RESULTS OF OBSERVATIONS

3.1. Flare activity of Cygnus X-3 in April and June, 2019

This Cygnus X-3 activity period included two flare states: in April–May (Trushkin et al., 2019) and in June, 2019 (Trushkin et al., 2020). In April, 2019 the multi-azimuth observation mode was for the first time used to study microquasars (Fig. 4). In June, 2019 Cygnus X-3 variability monitoring started. In the date intervals listed in

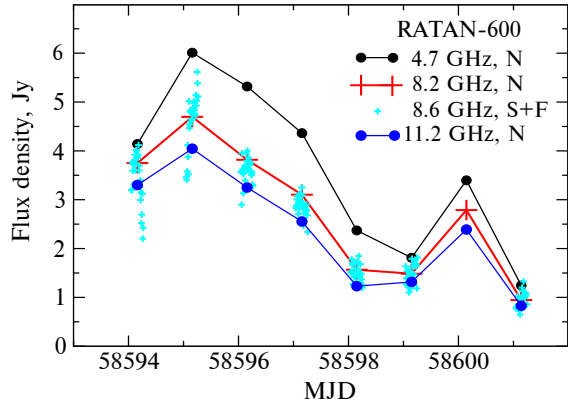


Figure 4. Daily measurements of Cygnus X-3 made in April 2019 with the Northern sector (the black, red, and blue crosses) and Southern sector with a flat reflector (crosses).

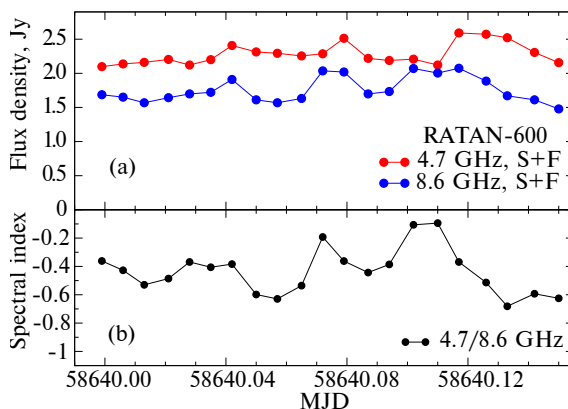


Figure 5. Intraday Cygnus X-3 variability according to measurements made on June 6, 2019. The bottom panel shows spectral index variations.

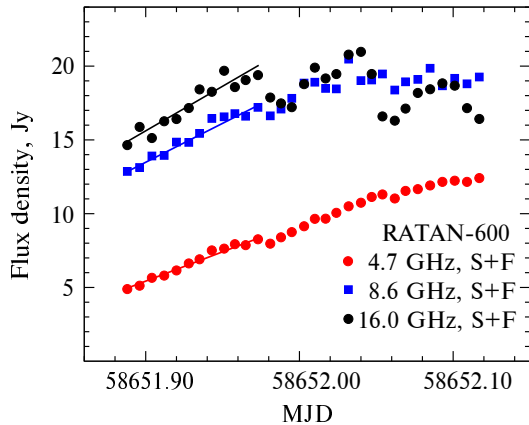
Table 2 intraday object flux measurements were made during daily observations at 4.7, 8.6, and 16 GHz. The resulting light curves are plotted in Figs. 5–7. It was during monitoring of 2019 radio flares that rapid (about 10 minutes) variability of Cygnus X-3.

Small flares were observed in early June. One of these flares coincided with a gamma-ray flare recorded by Fermi/LAT space observatory¹. Figure 5 shows the light curves and variations of spectral index during June 6, 2019 (MDJ 58640). As is evident from the figure, during small flares the spectrum was closer to flat, but then transformed into the usual optically thin spectrum.

¹ https://fermi.gsfc.nasa.gov/ssc/data/access/lat/msl_lc/source/Cygnus_X-3

Table 2. Table of 2019–2021 multi-azimuth observations

Observation dates	MJD	Reference sources
April 19–28, 2019	58592–58601	DR 21+3C 84
June 6–8, 2019, June 10, 2019	58640–58644	DR 21+3C 84
June 18–29, 2019	58652–58666	DR 21+3C 84
February 5–9, 2020, February 15–17, 2020	58884–58896	NGC 7027
December 25–30, 2021	59573–58579	NGC 7027

**Figure 6.** Multi-azimuth flux measurements of the microquasar Cygnus X-3 made with the Southern sector with a flat reflector during the first day of the flare, on June 18, 2019.

An important feature of our observations were Cygnus X-3 flux measurements at the early stage of the flare evolution. This event was recorded on June 18, 2019 and the stage of gradual increase of the source flux at all three frequencies—4.7, 8.6, and 16 GHz—was observed (Fig. 6).

The flux increase (up to the time of flare maximum) can be closely approximated by linear relation: $S_\nu \propto A(t - t_0)$, where t_0 is the time of the flare onset. We extrapolated this linear function to determine the ejection starting times 58561.75, 58561.60, and 58561.50 at 4.7, 8.6, and 16 GHz, respectively. We chose the same approximation interval in time for all three frequencies. Although the accuracy of such extrapolation is hardly better than one hour, it is worth pointing out the appreciable shift of the flare onset time from the high to low frequency, which can be easily explained in term of the model of a jet ejection rising in an absorbing shell.

According to the June 18, 2019 measurements, the $\alpha_{4.7/8.6}$ spectral index for 4.7–8.6 GHz frequencies changed from +1.6 to +0.7, whereas the $\alpha_{8.6/16.0}$ (8.6–16.0 GHz) spectral index was close to zero (Fig. 8). This result leads us to conclude that radio emission transformed from optically thick into optically thin state after the flare reached the maximum brightness level. Such spectral evolution is consistent with the radio-jet model with synchrotron self absorption operating at the beginning of the flare. Another possible scenario involves absorption by a mix of thermal and relativistic electrons in the jet. Absorption mechanisms are difficult to unambiguously separate without using widely separated measurement frequencies.

However, the fact that the spectral index is close to +2 indicates that the thermal absorption mechanism dominates over the self-absorption of relativistic electrons.

3.2. Flare activity of Cygnus X-3 in February, 2020

During the January 16, 2020 (MJD 58864) observations the flux decreased down to 5 mJy at 4.7 GHz and then remained very low over the next 12 days, as is usually the case during the period of the hypersoft X-ray state of the object (Koljonen et al., 2010). The first short-term event occurred on MJD 58876, when the flux increased to 100 mJy at 4.7 GHz. The second bright event with a flux of about 1 Jy was detected at MJD 58881.3, and the spectrum remained optically thick. On February 8, 2020 (MJD 58887.3) a giant flare started (Fig. 9). At

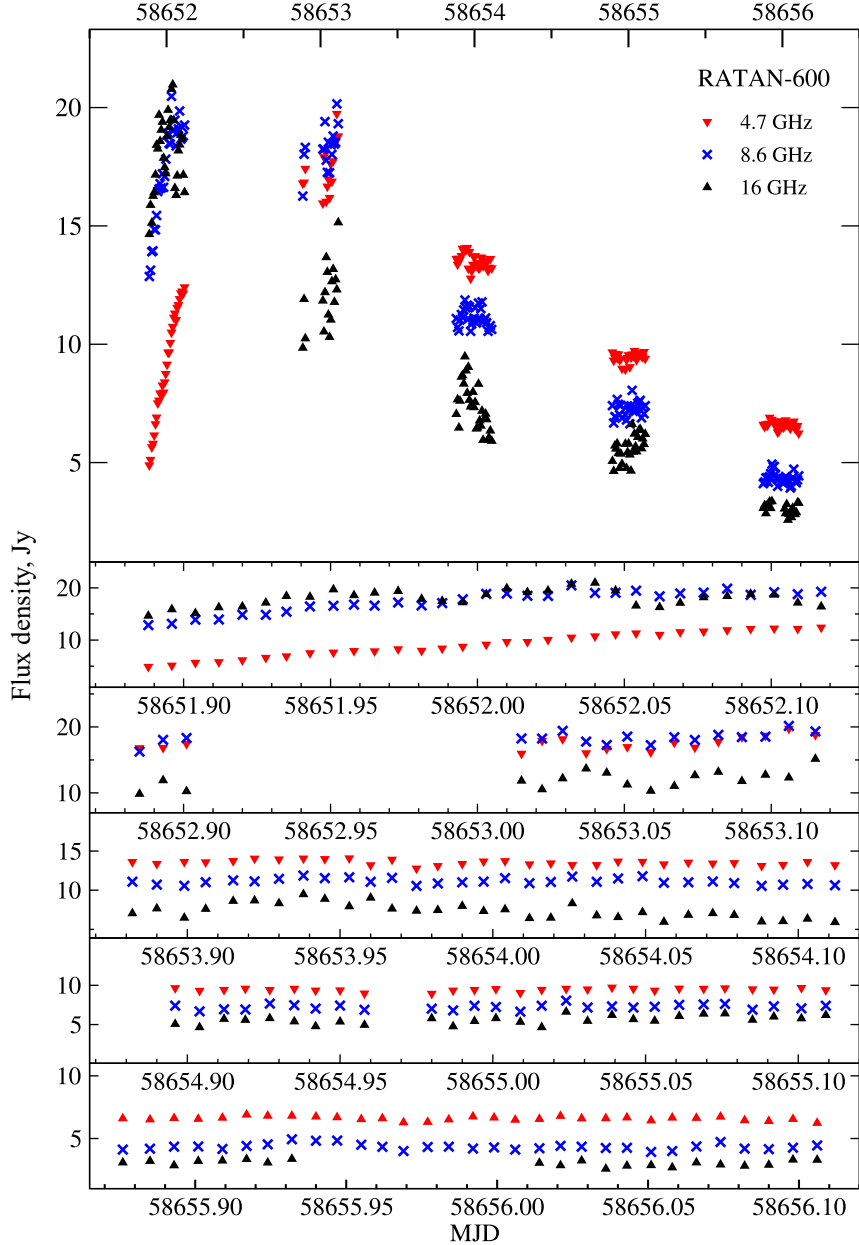


Figure 7. Cygnus X-3 light curves at three frequencies during five days: June 18–22, 2019.

that very time simultaneous observations were produced with AMI-LA radio telescope (Green and Elwood, 2020; Spencer et al., 2022).

Figure 10 shows the light curves and evolution of the two-frequency spectral index during MJD 58888. The flux increase during this optically thin flare was accompanied by the flattening of the spectrum typical for a flare onset, i.e., the spectral index decreased from -0.5 to -0.1 . Daily multi-frequency monitoring of microquasars and intraday measurements during

active states of Cygnus X-3 provide further insight into the relationship between the jet and the accretion disk in a microquasar. Synchrotron emission models allow estimating the size and brightness temperature of emission regions.

3.3. Flare activity of Cygnus X-3 in 2021

During the monitoring on July 31, 2021 we detected a giant flare from the microquasar

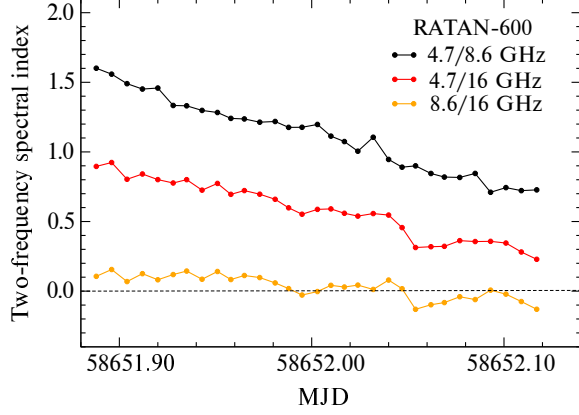


Figure 8. Evolution of the two-frequency spectral index during the June 18, 2019 measurements.

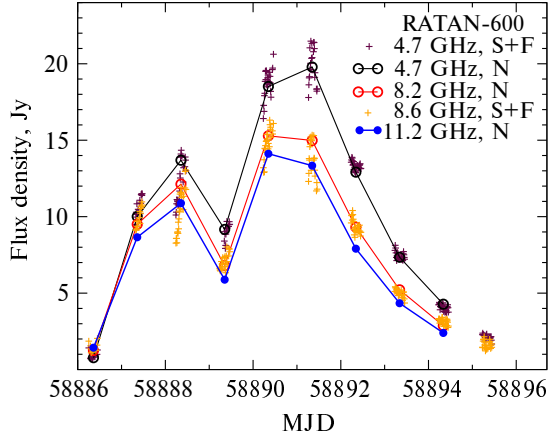


Figure 9. Daily measurements of Cygnus X-3 made in February, 2000 with the Northern sector with a flat reflector (crosses).

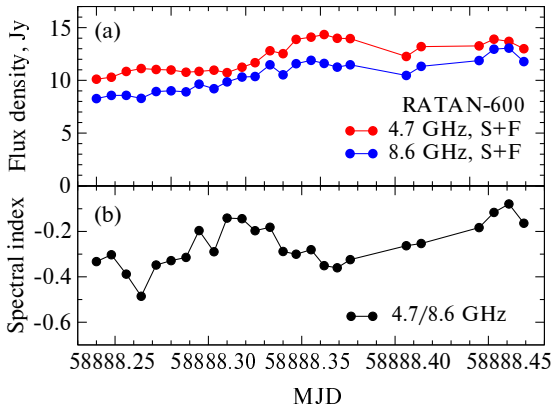


Figure 10. Variability of Cygnus X-3 on February 9, 2000 and evolution of spectral index.

Cygnus X-3 in the 1.2–30 GHz frequency interval. This flare was probably characterized by a single ejection and lasted for about two weeks. Like in most of the cases, the flare was accompanied by appreciable increase of γ -ray flux as it follows from the 0.1–300 GeV monitoring data for the object obtained from Fermi/LAT space observatory in MJD 59425.0. The gamma-ray event was recorded a little less than one day before we detected the 4.7 GHz radio flux maximum at MJD 59425.88. According to 15–50 keV Swift/BAT data², the active X-ray state continued and on October 18, 2021 (MJD 59505) we detected an unusual giant positive flare with the 4.7-GHz flux at maximum reaching almost 16 Jy (Fig. 11). This flare consisted of several consecutive ejections and ended after 45 days, on December 2 (MJD 59550).

According to Fermi observatory data, the October flare was also accompanied with γ -ray activity and lasted until November 13 (MJD 59531). On December 24, 2021 (MJD 59572.48) we detected a giant flare (Fig. 12), which was quite predictable because the microquasar remained in hypersoft state. And again, such spectrum is determined by optically thick (spectral index $\alpha = 1.6$) and optically thin ($\alpha = 0$) modes of the forming jets. The Cygnus X-3 then evolved into optically thin state with the usual spectral index $\alpha = -0.55$. We carried out four sets of observations in azimuths and found only small intraday variations of oscillations at 4.7 GHz (within 10%)(Fig. 13).

4. DISCUSSION

Radio flares are a good indicator of the formation process of a jet ejection and overall increase of activity in the Cygnus X-3 microquasar. The onset of the flare at the stage of rapid flux increase is of special interest because it provides an insight into how electrons responsible for synchrotron radio emission generated. In the case of the giant flare of June 18, 2019 we convincingly demonstrated that the 4.7, 8.6, and 16 GHz

² <https://swift.gsfc.nasa.gov/results/transients/CygX-3/>

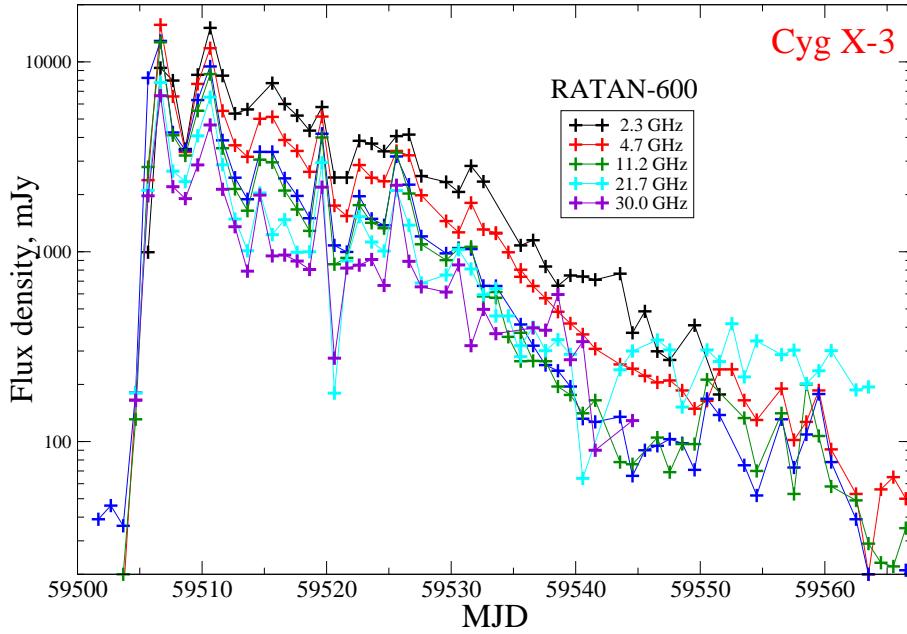


Figure 11. Light curves of Cygnus X-3 in October–November, 2021 based on daily monitoring data obtained with the Northern sector of RATAN-600 radio telescope.

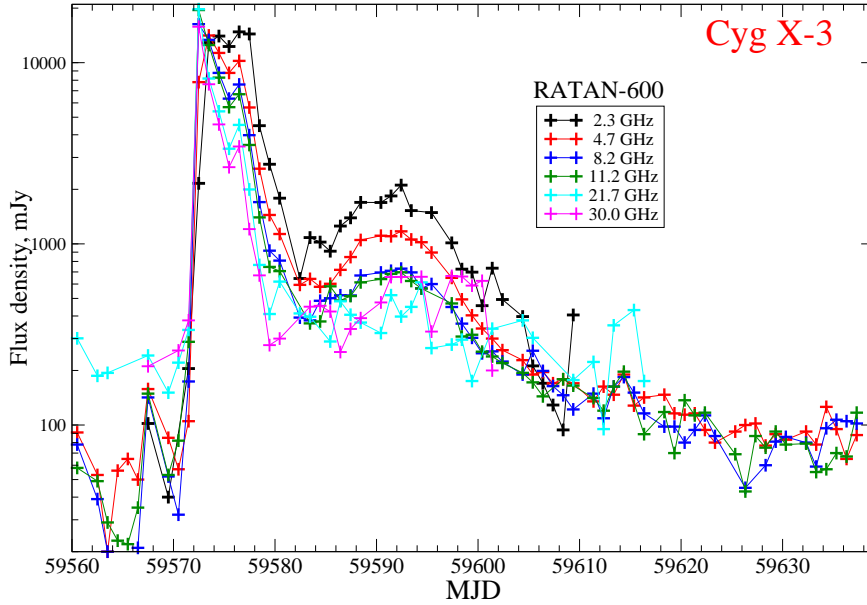


Figure 12. The Cygnus X-3 light curve at the beginning of a flare in December, 2021 according to monitoring data and multi-azimuth measurements.

fluxes of the flares increased linearly until reaching maximum levels and with a small delay for low frequencies.

Note that rapid evolution of optically thick radio emission imposes significant constraints on

the jet geometry. Indeed, after the flare onset volume clumps inside jets must usually expand in three dimensions in accordance with the classical model van der Laan (1966). However, such expansion may be exponential for jets with

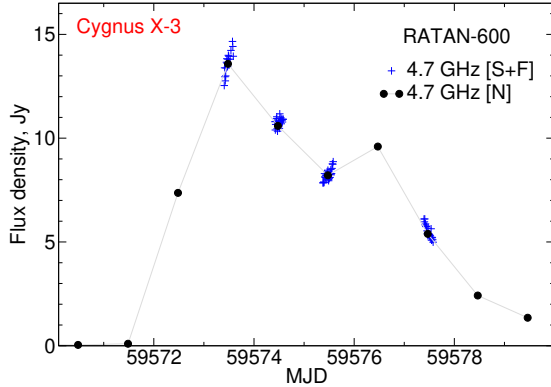


Figure 13. The 4.7-GHz Cygnus X-3 light curves according to measurements made with the Northern sector (the black dots) and Southern sector with a flat reflector in December, 2021.

conic geometry (Marti et al., 1992), when rather thin shock envelopes in jets may result in two-dimensional expansion.

The measured spectra were indicative of optically thick emission, which was probably associated with internal absorption by thermal electrons or with synchrotron self-absorption in accordance with Fender and Bright (2019). Smooth intraday radio flux variations was also detected at the stage of flare decay.

Here we focused only on the results of observations in the new mode for the context considered. We defer a more detailed analysis and the application of various models to the accompanying paper.

ACKNOWLEDGMENTS

Observations were performed with the equipment of RATAN-600 radio telescope of the Special Astrophysical Observatory of the Russian Academy of Sciences and supported by the Ministry of Science and Higher Education of the Russian Federation. We are sincerely grateful to the two reviewers for their constructive comments that helped to improve the paper.

FUNDING

Part of the observational data was exposed on the unique scientific facility the radio telescope RATAN-600 SAO RAS and the

data processing was supported under the Ministry of Science and Higher Education of the Russian Federation grant No. 075-15-2022-262 (13.MNPMU.21.0003).

CONFLICT OF INTEREST

The authors declare that there is no conflict of interest.

REFERENCES

- K. D. Aliakberov, M. G. Mingaliev, M. N. Naugol'naya, et al., *Bull. Spec. Astrophys. Obs.* **19**, 59 (1985).
- Y. Bhargava, A. R. Rao, K. P. Singh, et al., *Astrophys. J.* **849** (2), article id. 141 (2017).
- S. Corbel, G. Dubus, J. A. Tomsick, et al., *Monthly Notices Royal Astron. Soc.* **421** (4), 2947 (2012).
- R. Fender and J. Bright, *Monthly Notices Royal Astron. Soc.* **489** (4), 4836 (2019).
- R. Giacconi, P. Gorenstein, H. Gursky, and J. R. Waters, *Astrophys. J.* **148**, L119 (1967).
- D. A. Green and P. Elwood, *Research Notes Amer. Astron. Soc.* **4** (3), id. 36 (2020).
- P. C. Gregory, P. P. Kronberg, E. R. Seaquist, et al., *Nature* **239** (5373), 440 (1972).
- K. I. I. Koljonen, D. C. Hannikainen, M. L. McCollough, et al., *Monthly Notices Royal Astron. Soc.* **406** (1), 307 (2010).
- A. N. Korzhavin, V. N. L'vov, S. K. Tokhchukova, and S. D. Tsekmeister, *Astrophysical Bulletin* **67** (2), 225 (2012).
- J. Marti, J. M. Paredes, and R. Estalella, *Astron. and Astrophys.* **258**, 309 (1992).
- M. L. McCollough, C. R. Robinson, S. N. Zhang, et al., *Astrophys. J.* **517** (2), 951 (1999).
- J. C. A. Miller-Jones, K. M. Blundell, M. P. Rupen, et al., *Astrophys. J.* **600** (1), 368 (2004).
- M. Ott, A. Witzel, A. Quirrenbach, et al., *Astron. and Astrophys.* **284**, 331 (1994).
- R. E. Spencer, *ASP Conf. Ser.* **144**, 337 (1998).
- R. E. Spencer, M. Garrett, J. D. Bray, and D. A. Green, *Monthly Notices Royal Astron. Soc.* **512** (2), 2618 (2022).
- M. Tavani, A. Bulgarelli, G. Piano, et al., *Nature* **462** (7273), 620 (2009).
- S. Trushkin, M. McCollough, N. Nizhelskij, and P. Tsybulev, *Galaxies* **5** (4), 86 (2017).
- S. Trushkin, A. Shevchenko, N. Bursov, et al., in *Proc. All-Russian Conf. on Ground-Based Astronomy in Russia. 21st Century, Nizhny Arkhyz, Russia, 2020*, Ed. by I. I. Romanyuk, I. A. Yakunin, A. F. Valeev, and D. O. Kudryavtsev, (Spec. Astrophys. Obs. Russian Acad. Sci., Nizhnij Arkhyz, 2020), pp. 351–354 (2020).
- S. A. Trushkin, N. A. Nizhelskij, P. G. Tsybulev, and A. V. Shevchenko, *Astronomer's Telegram* **12510**, 1 (2019).

- P. G. Tsybulev, N. A. Nizhelskii, M. V. Dugin, et al., *Astrophysical Bulletin* **73** (4), 494 (2018).
- V. Tudose, R. P. Fender, M. A. Garrett, et al., *Monthly Notices Royal Astron. Soc.* **375** (1), L11 (2007).
- H. van der Laan, *Nature* **211** (5054), 1131 (1966).
- M. H. van Kerkwijk, P. A. Charles, T. R. Geballe, et al., *Nature* **355** (6362), 703 (1992).
- O. V. Verkhodanov, *ASP Conf. Ser.* **125**, 46 (1997).
- E. B. Waltman, R. L. Fiedler, K. J. Johnston, and F. D. Ghigo, *Astron. J.* **108**, 179 (1994).
- E. B. Waltman, R. S. Foster, G. G. Pooley, et al., *Astron. J.* **112**, 2690 (1996).
- A. A. Zdziarski, D. Malyshev, G. Dubus, et al., *Monthly Notices Royal Astron. Soc.* **479** (4), 4399 (2018).